

## TiO<sub>2</sub>-Zeolite Composite Modified Iron Nanoparticles for the Removal of Cr(VI) from Wastewater

P. ANJU ROSE PUTHUKKARA<sup>1D</sup>, T. SUNIL JOSE<sup>\*1D</sup> and S. DINOOP LAL<sup>1D</sup>

Department of Chemistry, St. Thomas College, Thrissur-680001, India

\*Corresponding author: E-mail: suniljosestc@gmail.com

Received: 24 December 2024;

Accepted: 11 February 2025;

Published online: 28 February 2025;

AJC-21926

Zero valent iron (Fe<sup>0</sup>) particles are significant in wastewater treatment because of their high reactivity, rapid kinetics, magnetic characteristics, and eco-friendliness. The primary drawbacks of Fe<sup>0</sup> nanoparticles are their rapid oxidation and aggregation. In this study, novel TiO<sub>2</sub>-zeolite composites with different percentages of TiO<sub>2</sub> were prepared and applied for Fe<sup>0</sup> stabilization. The TiO<sub>2</sub>-zeolite composite was synthesized using the sonication of components, subsequently employing the hydrothermal technique. Iron nanoparticles were included into the TiO<sub>2</sub>-zeolite composite using the wet impregnation method followed by liquid-phase reduction. For comparative study with TiO<sub>2</sub>-zeolite-Fe nanoparticles, TiO<sub>2</sub>-Fe and zeolite-Fe nanoparticles were also prepared. The characterization of TiO<sub>2</sub> and zeolite modified Fe nanoparticles were done by XRD, HRTEM, EDAX, FTIR and UV-visible spectroscopic techniques. The study evaluated the efficiency of prepared TiO<sub>2</sub>-Fe, zeolite-Fe and TiO<sub>2</sub>-zeolite-Fe nanoparticles to remove Cr(VI) from wastewater.

**Keywords:** Zero valent iron, Nanoparticles, TiO<sub>2</sub>, Zeolite, Hexavalent chromium.

### INTRODUCTION

The search for the most suitable material for the remediation of water pollutants is a never-ending process. Zero valent iron (Fe<sup>0</sup>) nanoparticle is an appropriate material for water remediation, however, the stability of Fe<sup>0</sup> nanoparticles is still a complicated issue. The rapid oxidation of the Fe<sup>0</sup> nanoparticles by reacting with air, moisture and non-targeted pollutants make them hard to handle. As per literature, TiO<sub>2</sub> can be used to retard the corrosion of metals and metal alloys [1]. In addition to this, TiO<sub>2</sub> is used for the adsorption of heavy metals [2], dyes [3], etc. and it is also used as a photocatalyst in various studies due to its chemical and photochemical stability, quantum confinement effect, strong resistance to acids and alkalis, large surface area to volume ratio along with low cost and low toxicity [4,5]. Serna-Galvis *et al.* [6] used TiO<sub>2</sub> as a photocatalyst to degrade the antibiotic oxacillin through hydroxyl radicals created in the valence band of the former through photogenerated holes. In their study, around 90% of the total organic carbon was removed by TiO<sub>2</sub> based photocatalysis. Previous studies show that Fe<sup>3+</sup> doping of TiO<sub>2</sub> reduces the TiO<sub>2</sub> band gap since Ti<sup>4+</sup> ions in the crystal lattice are substituted by Fe<sup>3+</sup> ions. The doping can shift the absorption of TiO<sub>2</sub> from the UV region to the visible region [7-9].

The charge carrier recombination rate gets reduced and the hydroxyl radical production has improved in Fe<sup>3+</sup> doped TiO<sub>2</sub> photocatalyst. This leads to the enhanced photocatalytic degradation of the organic pollutant under UV and visible light illumination [10]. The presence of metal ions/metal nanoparticles in the TiO<sub>2</sub> surface improves photocatalytic activity and can act as electron scavengers to catch the photogenerated electrons [11]. This property will be helpful for the stabilization of Fe<sup>0</sup> nanoparticles for more extended periods. Even though the TiO<sub>2</sub> nanoparticles can be used for water treatment, they show high colloidal stability in water and are difficult to separate and recover after use [12].

The disadvantages of TiO<sub>2</sub> nanoparticles can be overcome by immobilizing them on a suitable support, which helps easy removal and separation after use [13]. One of the inexpensive and non-toxic supports for metal/metal oxide nanoparticles are zeolites. Zeolites are three-dimensional aluminosilicate frameworks that show high surface area, abundant surface active sites for adsorption and excellent ion exchange capacity. More than that, it is resistant to the attack of hydroxyl radicals and effective even after recycling many times. It is important to note that the negative surface charges of the zeolites help them to show a high affinity towards cationic species [14]. The modification of zeolite by TiO<sub>2</sub> has been studied over the years. Several

methods were used to establish TiO<sub>2</sub> nanoparticles on the surface of the zeolite. Sun *et al.* [15] produced TiO<sub>2</sub> nanoparticles supported on natural zeolite by the hydrolysis of TiCl<sub>4</sub>. Jan *et al.* [16] prepared TiO<sub>2</sub>-zeolite composite by wetness impregnation method in which the components are mixed, sonicated and finely sprayed on the hot glass plate. In another study, Mirzaei *et al.* [17] synthesized NaX zeolite stabilized MgO-TiO<sub>2</sub> nanocomposite using the ultrasound-assisted dispersion method. The MgO and TiO<sub>2</sub> nanoparticles were mixed with NaX zeolite in water followed by sonication, stirring, drying and calcination, giving NaX/MgO-TiO<sub>2</sub> nanocomposite.

In present study, TiO<sub>2</sub>-zeolite composite was prepared by the hydrothermal method and these composites were used to stabilize Fe<sup>0</sup> nanoparticles. The major objectives of the study are (i) synthesis of TiO<sub>2</sub>-zeolite composite (T-Z) with varying TiO<sub>2</sub> dosage; (ii) synthesis of Fe<sup>0</sup> nanoparticles supported on TiO<sub>2</sub> nanoparticles, natural zeolite and TiO<sub>2</sub>-zeolite composites; (iii) characterization of the synthesized composites and nanoparticles; and (iv) its application to removal of Cr(VI) in wastewater by synthesized composites and nanoparticles.

## EXPERIMENTAL

### Synthesis of TiO<sub>2</sub>-zeolite stabilized Fe nanoparticles:

The TiO<sub>2</sub>-zeolite composite was synthesized by depositing TiO<sub>2</sub> nanoparticles on the zeolite surface. At first, washed the natural zeolite to remove organic impurities present in it. This is attained through sonication of zeolite in water followed by calcination at 600 °C for 6 h in a muffle furnace. The subsequent cooling at room temperature and powdering using pestle and mortar provide refined zeolite particles. The TiO<sub>2</sub>-zeolite composite was prepared by mixing specific weight percentages of TiO<sub>2</sub> nanoparticles with zeolite powder in 10% aqueous ethanolic medium. This solution was sonicated using a probe sonicator for 0.5 h and kept at 120 °C for 6 h in a Teflon-lined stainless steel autoclave. After that, the autoclave was cooled down at room temperature and washed with demineralized water. The TiO<sub>2</sub>-zeolite composite was further calcinated at 600 °C for 6 h and powdered using pestle and mortar. The 25% TiO<sub>2</sub> nanoparticles loaded zeolite (25-T-Z) and 50% TiO<sub>2</sub> nanoparticles loaded zeolite (50-T-Z) were synthesized by maintaining the TiO<sub>2</sub> and zeolite particles ratio at 25:75 and 50:50, respectively.

The TiO<sub>2</sub>-zeolite-Fe composite was prepared by the wet impregnation method. For this, FeCl<sub>3</sub>.6H<sub>2</sub>O (1 g) was dissolved in 10 mL of water and added 0.5 g of T-Z into it. The solution was stirred for 0.5 h and evaporated the solvent using a hot plate. The obtained material was powdered, weighed and redispersed in 10 mL of water and stirred 0.5 h under the nitrogen atmosphere. NaBH<sub>4</sub> solution was prepared by dissolving 0.5 g in 50 L of water and added dropwise to the solution. The appearance of a black precipitate indicates the formation of Fe<sup>0</sup> nanoparticles in the TiO<sub>2</sub>-zeolite matrix. The precipitate was collected by vacuum filtration, washed with acetone, lyophilized and stored in airtight vials. In the synthesis of 25-T-Z-Fe, the 25-T-Z composite was used and for 50-T-Z-Fe preparation, the composite 50-T-Z was used. A similar procedure was followed

to prepare T-Fe and Z-Fe nanoparticles in which TiO<sub>2</sub> nanoparticles and zeolite were used as stabilizing agents.

**Cr(VI) removal studies:** The concentration of Cr(VI) in wastewater was determined using the USEPA 7196A method. For the Cr(VI) removal study, a specific amount of iron-based nanoparticles was added into 10 mL of Cr(VI) solution of the desired concentration. After sonication for a previously determined time, the solution was centrifuged and 9.5 mL of Cr(VI) solution was transferred into a 10 mL vial. A 0.2 mL of diphenylcarbazide was added and mixed gently followed by the addition of 10% H<sub>2</sub>SO<sub>4</sub> to obtain the solution with pH 2 and diluted to 10 mL using demineralized water. The solution was kept for 5 to 10 min for complete colour development. After measuring the absorbance, chromium (mg/L) present in the solution was determined using the calibration curve.

$$\text{Removal efficiency (\%)} = \frac{C_0 - C_t}{C_0} \times 100$$

where C<sub>0</sub> and C<sub>t</sub> were the initial and final Cr(VI) concentrations in the aqueous solution, respectively.

Various parameters examined in this study for Cr(VI) removal were nanoparticle dosage (0.4-1.0 g/L), initial concentration of Cr(VI) (1-7 mg/L), initial pH of solution (4-10) and contact time (10-40 min). The pH of the solution was adjusted using 1.0 M NaOH and 1.0 M H<sub>2</sub>SO<sub>4</sub>. All the experiments were performed with a duplicate.

**Characterization:** The prepared nanoparticles were lyophilized using Operon FDU 7003 lyophiliser instrument. The characteristics of TiO<sub>2</sub> nanoparticles, zeolite and TiO<sub>2</sub>-zeolite composites and corresponding iron nanoparticles were examined by HRTEM, UV-visible spectroscopy, EDAX, XRD and FTIR. UV-visible spectrometer UV-2600, Shimadzu, Japan, was used to study the absorbance of TiO<sub>2</sub> nanoparticles, zeolite and TiO<sub>2</sub>-zeolite composites and corresponding iron nanoparticles. Fourier transform infrared spectra of the prepared composite and corresponding Fe nanoparticles were investigated through Spectrum Two Fourier transform infrared spectrometer (FTIR, Perkin-Elmer, USA). A Jeol 6390LA/OXFORD XMX N instrument was used for the elemental analysis of T-Fe, Z-Fe, 50-T-Z and 50-T-Z-Fe nanoparticles. Particle size and morphology of the prepared compounds were analyzed using Jeol/JEM 2100 High-resolution transmission electron microscopy (HRTEM) and the XRD data were collected using PANalytical Aeries X-ray diffractometer using CuKα radiation of wavelength (λ = 0.15406 nm) in the scan range 2θ = 5-90°. The absorbance of the solution was measured using a UV-visible spectrophotometer (Shimadzu UV 1800) instrument.

## RESULTS AND DISCUSSION

### Characterization of the prepared materials

**XRD studies:** X-ray diffractogram of TiO<sub>2</sub> nanoparticles, zeolite powder, 25% TiO<sub>2</sub> loaded zeolite composite and 50% TiO<sub>2</sub> loaded zeolite composite is shown in Fig. 1a. The powder XRD pattern of TiO<sub>2</sub> exhibited strong diffraction peaks at 2θ = 25.70° (101), 38.30° (004), 48.49° (200), 54.49° (105) and 55.44° (211) corresponding to the anatase phase of TiO<sub>2</sub> [18].

The diffraction peaks observed at  $2\theta$  69.31° (031) and 70.50° (112) indicated the presence of the rutile phase of TiO<sub>2</sub> in lower percentages (JCPDS card no. 98-018-6186). Anatase TiO<sub>2</sub> nanoparticles show superior photocatalytic property compared to rutile TiO<sub>2</sub>. In the XRD spectrum of zeolite, the peaks shown at 30.30°, 27.40°, 24.30°, 22.00° and 10.50° corresponds to the clinoptilolite zeolite [19,20]. The XRD peaks of 25-T-Z and 50-T-Z have a similar pattern of TiO<sub>2</sub> and zeolite, with a slight shift in the XRD peaks. With the increase in TiO<sub>2</sub> dosage, the peaks of zeolite were decreased drastically. This indicates that zeolites are covered with TiO<sub>2</sub> nanoparticles completely. Fig. 1b shows the XRD pattern of Fe nanoparticles stabilized on the TiO<sub>2</sub> nanoparticles, zeolite, 25-T-Z and 50-T-Z composites. The XRD peak at 45.40° indicates (110) plane of the zero valent iron, which is present in all the four Fe nanoparticles [21]. The intense peak at 31.70° corresponds to the (104) plane of  $\alpha$ -Fe<sub>2</sub>O<sub>3</sub> [22]. The other peaks in the T-Fe, Z-Fe, 25-T-Z-Fe and 50-T-Z-Fe nanoparticles were that of the corresponding stabilising agent, TiO<sub>2</sub> and zeolite, with a slight shift in their peak position.

The high peak intensity of Fe<sup>0</sup> in 50-T-Z-Fe and T-Fe nanoparticles indicates the efficient stabilization of Fe<sup>0</sup> in these matrices, which is mainly due to the involvement of TiO<sub>2</sub> nanoparticles. Typically, TiO<sub>2</sub> nanoparticles are photocatalytically active in the UV region. However, its activity can be shifted to the visible region through the doping of Fe [23]. Electrons get excited to the conduction band of TiO<sub>2</sub> from its valence band when exposed to UV radiation, which leads to the formation of electron-hole pairs within the system. The lifetime of these excited electron-hole pair determines the photochemistry of TiO<sub>2</sub>. Photocatalytic activity of TiO<sub>2</sub> is minimized as the excited electrons in the conduction band recombines with the holes in the valence band. This charge recombination could be minimized by coupling TiO<sub>2</sub> with materials that can accept the electrons from the conduction band. According to Petala *et al.* [11], the iron oxide shell of the Fe<sup>0</sup> nanoparticles can act as electron trappers and accept the photoexcited electron from the conduction band of TiO<sub>2</sub>, thereby reducing Fe<sup>3+</sup> to Fe<sup>2+</sup>. The interaction

between TiO<sub>2</sub> and Fe retard the thicker iron oxide layer formation and gives longer reactivity of Fe<sup>0</sup> nanoparticles in TiO<sub>2</sub> matrices. The incorporation of zeolite enhanced the efficiency of TiO<sub>2</sub> nanoparticles, which may be due to the more dispersibility of TiO<sub>2</sub> nanoparticles in the zeolite matrix. Previous studies show that the photocatalytic activity of TiO<sub>2</sub> can be enhanced using zeolite as a supporting agent [24]. In case of 50-T-Z-Fe, the TiO<sub>2</sub> nanoparticles were more dispersed in zeolite matrix and may show high surface area. This leads to the improved stabilization Fe<sup>0</sup> in 50-T-Z-Fe nanoparticles.

**Morphological studies:** Fig. 2 represents the HRTEM images and SAED patterns of 50-T-Z and 50-T-Z-Fe, respectively. As shown in Fig. 2a, the TiO<sub>2</sub> nanoparticles were deposited on the surface of the zeolite. The particle size of TiO<sub>2</sub> ranges between 20-35 nm with an average particle size of 25 nm and the size of zeolite particles is around 150 nm. The 50-T-Z nanomaterials show the crystalline property, which is evident from the SAED pattern. Fig. 2b envisages that the Fe<sup>0</sup> nanoparticles with particle size below 20 nm were deposited on the surface of TiO<sub>2</sub> nanoparticles. The Fe nanoparticles exhibit a shell of iron oxide which may arise due to the oxidation of nanoparticles. The SAED pattern of 50-T-Z-Fe shows that the nanoparticles display crystalline properties similar to the 50-T-Z.

EDAX spectra and mapping of T-Fe, Z-Fe, 50-T-Z and 50-T-Z-Fe nanoparticles are shown in Figs. 3a-d and 4a-d, respectively. EDAX spectra confirmed the presence of respective elements in the prepared nanoparticles; for example, T-Fe contains Ti, O and Fe, Z-Fe contains Al, Si, O and Fe, 50-T-Z contains Al, Si, O and Ti and 50-T-Z-Fe contains Al, Si, O, Ti and Fe elements. As shown in Fig. 3, the percentage of oxygen is less in 50-T-Z-Fe compared to T-Fe and Z-Fe, which shows that 50-T-Z protects Fe<sup>0</sup> more efficiently than TiO<sub>2</sub> and zeolite. In accordance with the EDAX spectra, the atomic weight percentage of Fe in T-Fe, Z-Fe and 50-T-Z-Fe nanoparticles were 15%, 16% and 20%, respectively. The EDAX mapping of prepared nanoparticles gives information about the distribution of Fe nanoparticles in TiO<sub>2</sub>, zeolite, 25-T-Z and 50-T-Z matrices. The iron nanoparticles were uniformly distributed in TiO<sub>2</sub> and

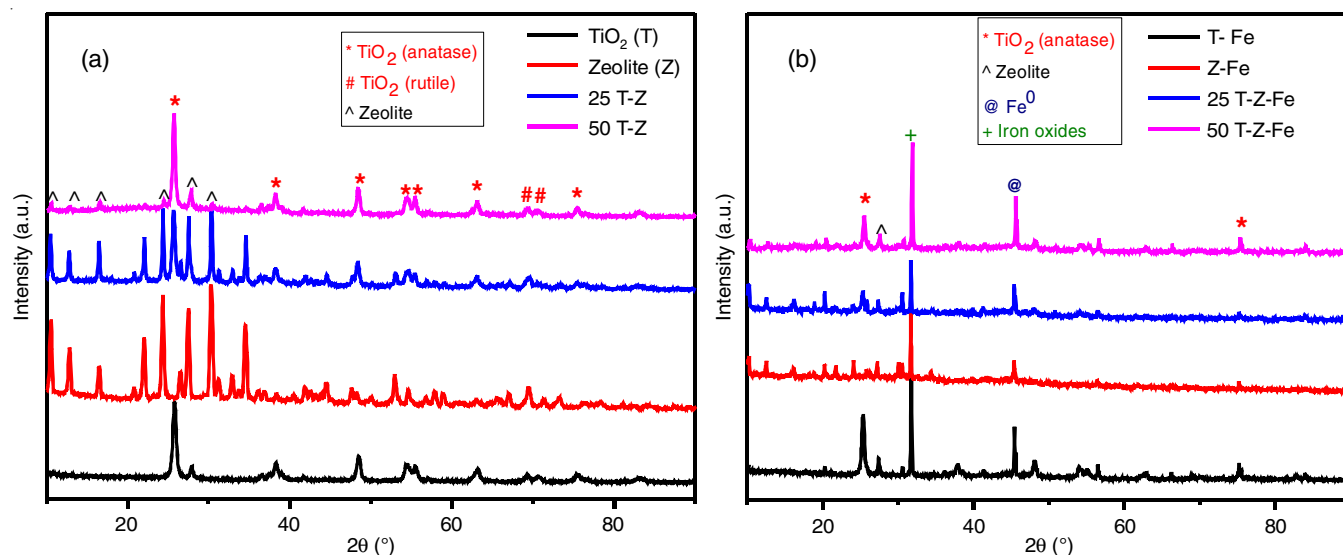


Fig. 1. XRD pattern of (a) TiO<sub>2</sub> nanoparticles, zeolite, 25-T-Z and 50-T-Z composite and (b) T-Fe, Z-Fe, 25-T-Z-Fe and 50-T-Z-Fe nanoparticles

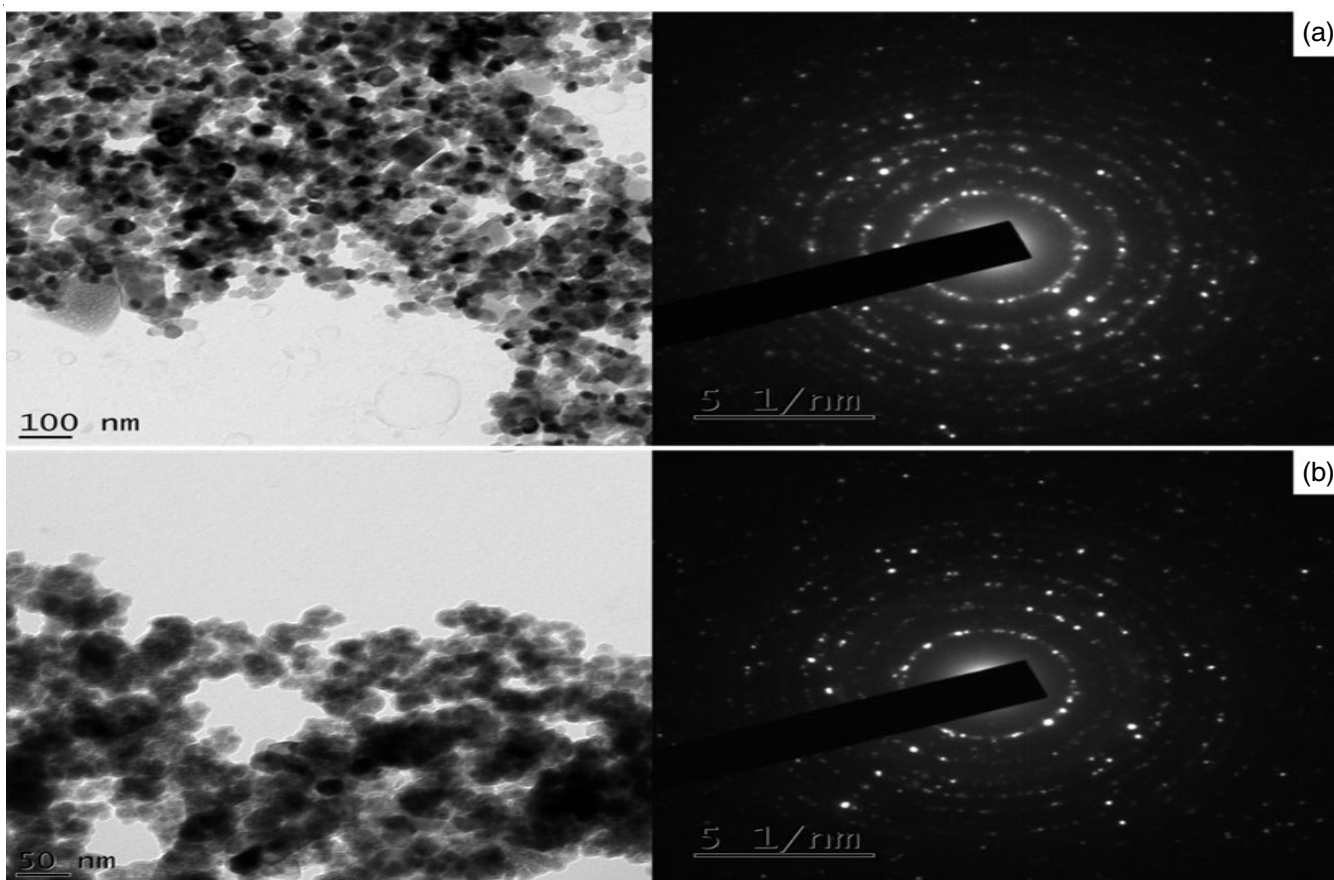


Fig. 2. HRTEM image SAED pattern of 50-T-Z (a) and 50-T-Z-Fe (b) nanoparticles

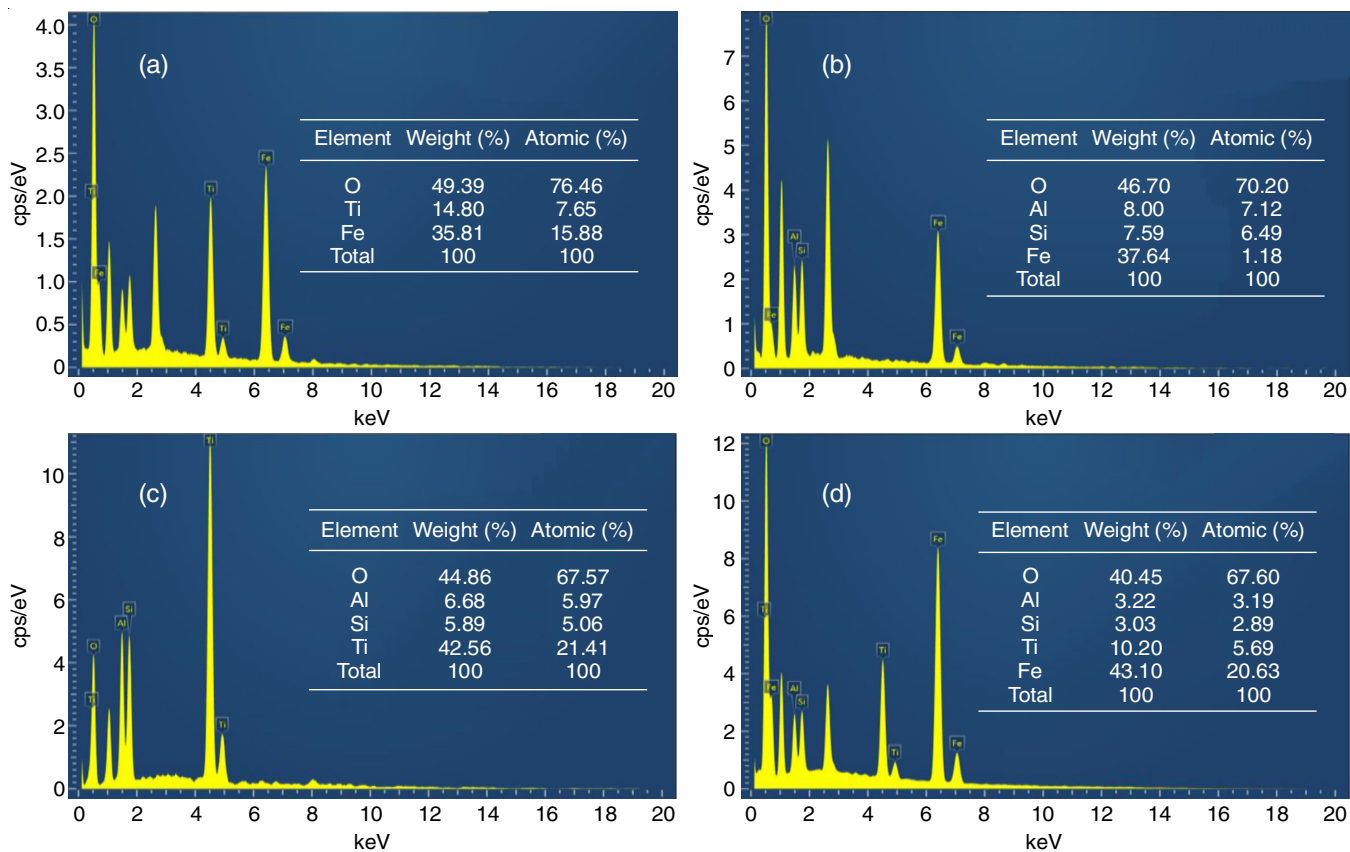


Fig. 3. EDAX spectra of (a) T-Fe, (b) Z-Fe, (c) 50-T-Z and (d) 50-T-Z-Fe

50-T-Z surfaces. In case of Z-Fe, the Fe nanoparticles were more present in zeolite channel/cavities than surfaces as indicated by the reduced intensity of Fe in Z-Fe nanoparticles (Fig. 4b).

**FTIR spectral studies:** Fig. 5 represents the FTIR spectra of T-Fe, Z-Fe, 25-T-Z-Fe and 50-T-Z-Fe nanoparticles and their corresponding stabilizing materials. The interaction between Fe<sup>0</sup> and stabilizing materials were established using FTIR measurements. Fig. 5a represents the FTIR spectra of TiO<sub>2</sub> and T-Fe nanoparticles. The peak centred at 3479 cm<sup>-1</sup>, belonging

to the stretching vibration of the -OH group due to the absorption of moisture from the atmosphere. The peak at 730 cm<sup>-1</sup> corresponding to the O-Ti-O bonding of TiO<sub>2</sub> anatase nanoparticles shifted to 694 cm<sup>-1</sup> in T-Fe nanoparticles [25]. This confirms the incorporation of Fe in TiO<sub>2</sub> lattice since the red shift is a sign of structural defect in TiO<sub>2</sub> lattice. In Fig. 5b, the existence of zeolite can be confirmed by the peaks between 850-400 cm<sup>-1</sup> [26]. The shift in peak position from 1365 cm<sup>-1</sup> to 1350 cm<sup>-1</sup> suggests the interaction of Fe nanoparticles with

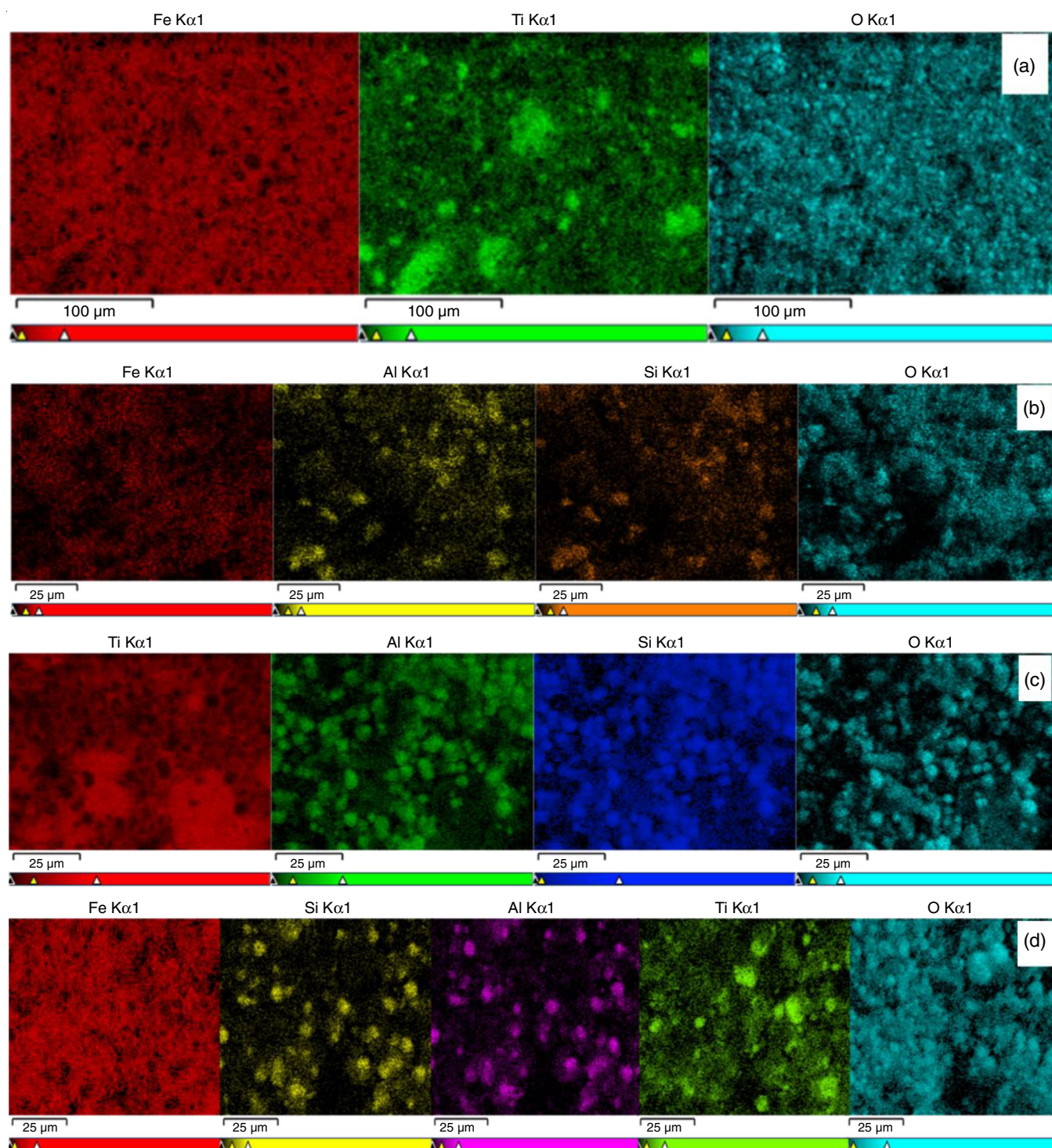


Fig. 4. EDAX mapping of (a) T-Fe, (b) Z-Fe, (c) 50-T-Z and (d) 50-T-Z-Fe

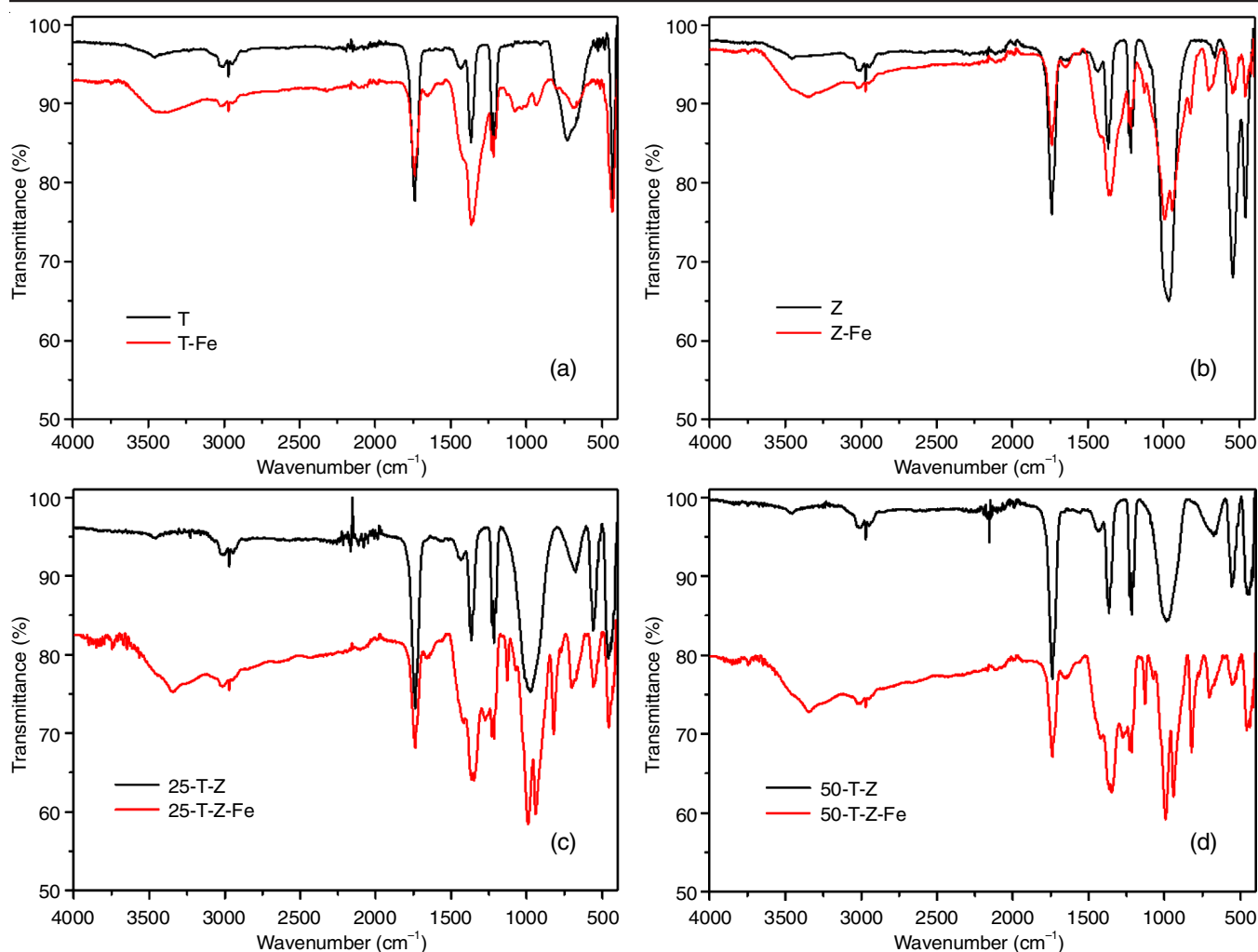


Fig. 5. FTIR spectra of (a) TiO<sub>2</sub> and T-Fe nanoparticles, (b) zeolite and Z-Fe nanoparticles, (c) 25-T-Z and 25-T-Z-Fe nanoparticles and (d) 50-T-Z and 50-T-Z-Fe nanoparticles

zeolite. The peak centred around 980 cm<sup>-1</sup> is due to the vibration of Si-O or Al-O of the zeolite is split into two peaks due to the replacement of Si with Fe during the Fe deposition. The zeolite peaks at 663 cm<sup>-1</sup> were blue-shifted to 696 cm<sup>-1</sup> in Z-Fe nanoparticles. This also supports the interaction of zeolite with Fe<sup>0</sup> nanoparticles. A similar trend has also been observed in 25-T-Z-Fe and 50-T-Z-Fe nanoparticles too. The FTIR spectra of 25-T-Z and 50-T-Z exhibit the peaks of TiO<sub>2</sub> and zeolite. The introduction of Fe shifted the peaks to higher/lower wavenumber.

**UV-visible spectral studies:** TiO<sub>2</sub> exhibited its characteristic absorption maxima in the UV region as observed by UV-visible spectroscopy (Fig. 6). The absorbance spectrum of zeolite also reveals its characteristic absorbance in the UV region of spectra. A considerable shift in peak intensity and position occurred in the absorption spectra of TiO<sub>2</sub> and zeolite with the incorporation of Fe. The presence of Fe in TiO<sub>2</sub>, decreased the intensity of absorption of the latter in the UV region and enhanced the absorption of TiO<sub>2</sub> in the visible region. This red shift in the peak position of TiO<sub>2</sub> in T-Fe is depicted in Fig. 6a. On the other hand, the UV spectra of Z-Fe composite displayed enhanced absorption intensity in UV and the visible

region compared to that of pristine zeolite. All these observations support the existence of molecular interaction between TiO<sub>2</sub> as well as zeolite with Fe. The presence of Fe extended the absorption of TiO<sub>2</sub> and zeolite to the visible region. Similar reconstructions were observed in the absorption bands of T-Z composites (25 T-Z-Fe and 50 T-Z-Fe) with the association of Fe. The extension of absorption of TiO<sub>2</sub>, zeolite and T-Z to visible region in the presence of Fe also suggests the possibility of these composites to exhibit their photocatalytic activity in the visible region too.

**Removal of chromium(IV) studies:** The Cr(VI) removal studies have been performed using T-Fe, Z-Fe, 25-T-Z-Fe and 50-T-Z-Fe nanoparticles. The results show that 25-T-Z-Fe and 50-T-Z-Fe nanoparticles exhibit the highest removal efficiency compared to T-Fe and Z-Fe nanoparticles (Fig. 7). This indicates the presence of more Fe<sup>0</sup> in 25-T-Z-Fe and 50-T-Z-Fe than T-Fe and Z-Fe nanoparticles. The improved efficiency of Z-Fe over T-Fe may be due to the adsorption of Cr(VI) ions onto the vacant cavities/channels of zeolite. The synergetic activity of zeolite and TiO<sub>2</sub> significantly reduced the oxidation probability of Fe<sup>0</sup> nanoparticles and enhanced the adsorption properties of 25-T-Z-Fe and 50-T-Z-Fe nanoparticles. The existence of

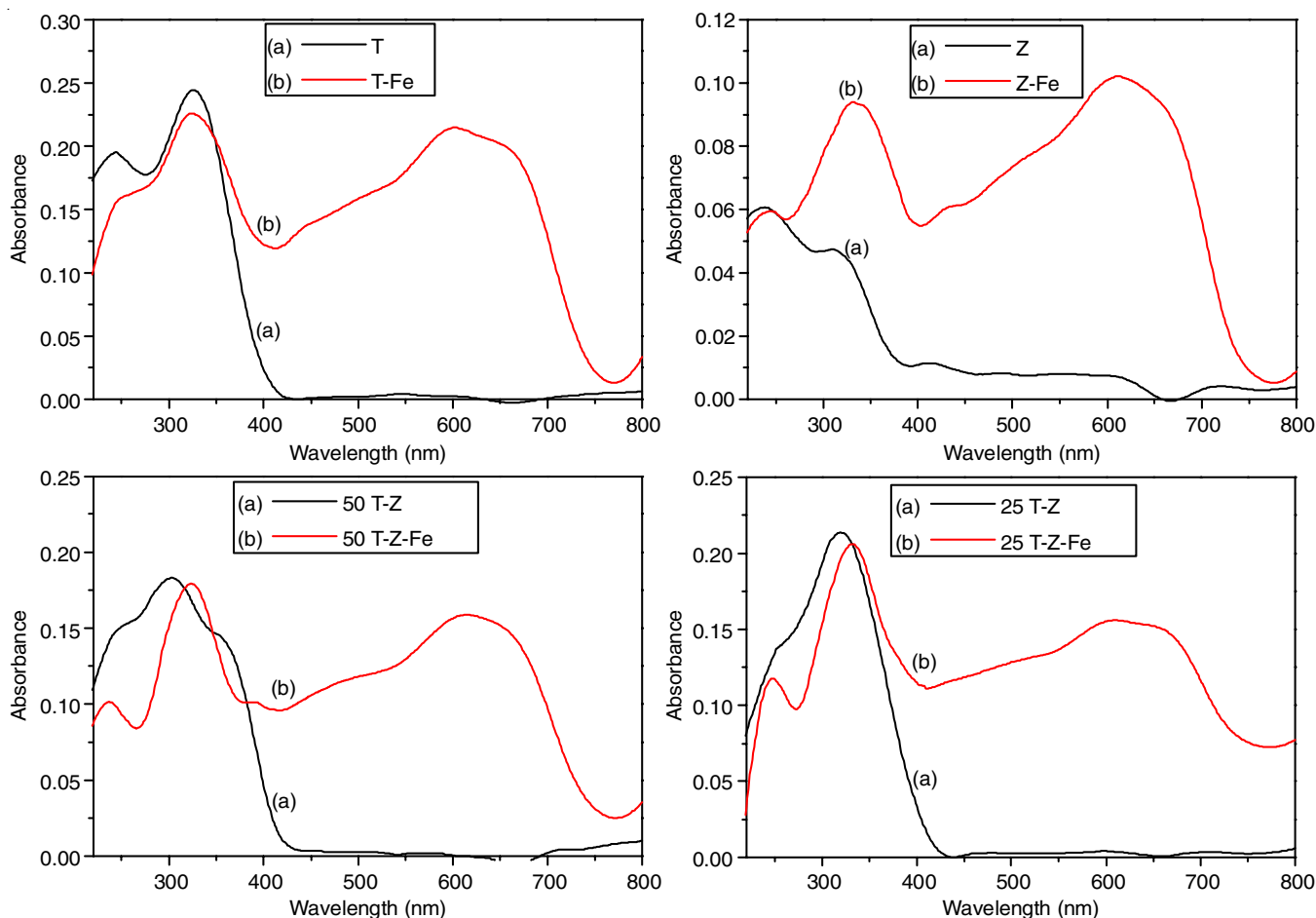


Fig. 6. UV-visible spectra of T-Fe, Z-Fe, 25-T-Z-Fe and 50-T-Z-Fe nanoparticles in comparison with TiO<sub>2</sub> and zeolite

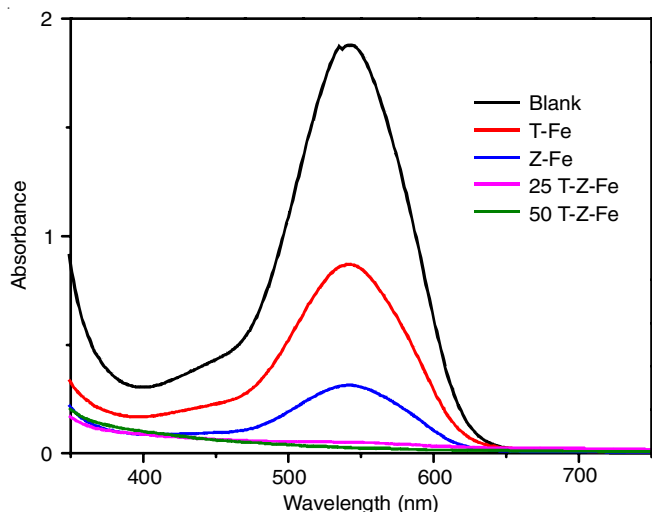


Fig. 7. UV-visible spectra of Cr(VI) after treating with T-Fe, Z-Fe, 25-T-Z-Fe and 50-T-Z-Fe nanoparticles

TiO<sub>2</sub> nanoparticles also added some effect on Cr(VI) removal. TiO<sub>2</sub> nanoparticles exhibit photocatalytic activity in the visible region along with the UV region due to the doping of Fe [23]. So, the absorption of visible light followed by the generation of electrons and holes also influenced the reduction of Cr(VI). The photogenerated electrons reduce the Cr(VI) to Cr(III) through redox reactions to some extent [27]. Some of the

photogenerated electrons were trapped by the iron oxide shell and regenerated after the Cr(VI) reduction [11]. The synergistic photocatalytic effect of TiO<sub>2</sub> and zeolite adsorption significantly improved the Cr(VI) removal in 25-T-Z-Fe and 50-T-Z-Fe systems.

**Effect of dosage:** Fig. 8a represents the effect of nanoparticles dosage on the Cr(VI) removal using T-Fe, Z-Fe, 25-T-Z-Fe and 50-T-Z-Fe nanoparticles. The nanoparticles dosage varied between 0.4 g/L to 1 g/L maintaining the initial Cr(VI) concentration at 5 mg/L and with a contact time of 15 min. The results show the highest removal efficiency in 25-T-Z-Fe nanoparticles along with 50-T-Z-Fe nanoparticles and the lowest Cr(VI) removal efficiency exhibited by T-Fe nanoparticles. While using 0.8 g/L of nanoparticles, the T-Fe, Z-Fe, 25-T-Z-Fe and 50-T-Z-Fe nanoparticles show 78%, 89%, 95% and 93% of Cr(VI) removal efficiency, respectively. The removal efficiency increased with the increase in nanoparticles dosage which is attributed to the high surface area and high surface active sites of prepared nanoparticles along with the rise in nanoparticles dosage. After the dosage of 0.8 g/L, the removal efficiency does not improve significantly. This may be due to the aggregation of nanoparticles.

**Effect of initial concentration of Cr(VI) solution:** The effect of the initial concentration of nanoparticles on the removal of Cr(VI) from water is shown in Fig. 8b. The nanoparticles dosage and contact time during the study were kept constant

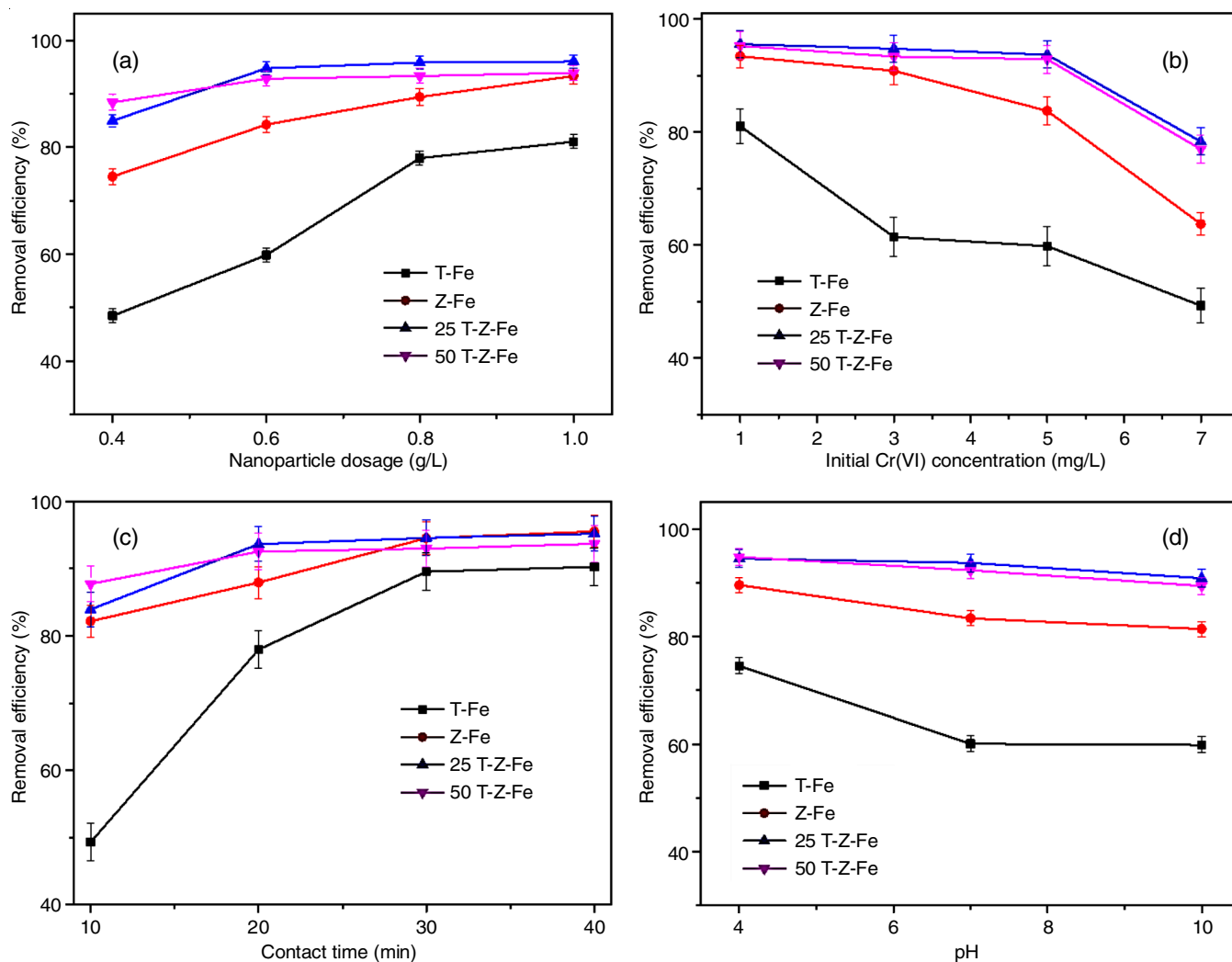


Fig. 8. (a) Effect of nanoparticle dosage, (b) effect of initial concentration of Cr(VI), (c) effect of contact time and (d) effect of pH on Cr(VI) removal using T-Fe, Z-Fe, 25-T-Z-Fe and 50-T-Z-Fe nanoparticles

at 0.6 g/L and 15 min, respectively. The results show that the removal efficiency decreased drastically with an increase in Cr(VI) concentration. The highest removal efficiency was exhibited in 1 mg/L Cr(VI) solution and the lowest by 7 mg/L Cr(VI) solution. In 1 mg/L solution, the T-Fe, Z-Fe, 25-T-Z-Fe and 50-T-Z-Fe nanoparticles exhibit 81%, 93%, 95% and 95% removal efficiency which is reduced to 49%, 63%, 78% and 76% at 7 mg/L solutions. This is due to the increase in the ratio between pollutant molecules and nanoparticle dosage, which leads to the decrease in the availability of surface active sites for the reduction of Cr(VI) ions.

**Effect of contact time:** As shown in Fig. 8c, the effect of contact time on Cr(VI) removal has been studied by keeping nanoparticles dosage (0.6 g/L) and initial Cr(VI) concentration (5 mg/L) constant. The results show that the 25-T-Z-Fe and 50-T-Z-Fe nanoparticles attained the maximum removal efficiency within 20 min of reaction time. However, in case of T-Fe and Z-Fe nanoparticles, 30 min is needed to attain the maximum removal efficiency, which indicates that 25-T-Z-Fe and 50-T-Z-Fe nanoparticles reacted more actively with Cr(VI) ions than T-Fe and Z-Fe nanoparticles. At 40 min of contact time the T-

Fe, Z-Fe, 25-T-Z-Fe and 50-T-Z-Fe nanoparticles display 77%, 87%, 93% and 92% Cr(VI) removal efficiency.

**Effect of pH:** The results demonstrate that the pH has little effect on Cr(VI) removal for Z-Fe, 25-T-Z-Fe and 50-T-Z-Fe nanoparticles (Fig. 8d). However, the removal efficiency reduced significantly in T-Fe nanoparticles from acidic to basic pH. The high removal efficiency in low pH may be due to the high degree of protonation of prepared nanoparticles and the shredding of iron oxide shell in the prepared Fe<sup>0</sup> nanoparticles.

## Conclusion

In this study, TiO<sub>2</sub>-zeolite composite was used to stabilize Fe<sup>0</sup> nanoparticles. The TiO<sub>2</sub>-zeolite composite was prepared by sonication followed by the hydrothermal method. The Fe<sup>3+</sup> was incorporated in TiO<sub>2</sub>-zeolite composite by wet impregnation and synthesized Fe<sup>0</sup> nanoparticles by liquid-phase reduction. The characterization of TiO<sub>2</sub>-zeolite composite and T-Z-Fe nanoparticles have been done by XRD, FTIR, UV-visible spectroscopy, EDAX and HRTEM. In the prepared nanoparticles, 25-T-Z-Fe and 50-T-Z-Fe nanoparticles show more removal efficiency for Cr(VI) compared to T-Fe and Z-Fe nanoparticles. The

removal efficiency increases with increasing nanoparticle dosage and contact time and decreasing the initial concentration of the pollutant and pH of the solution. This study envisages that among the prepared TiO<sub>2</sub>/zeolite nanoparticles, 25-T-Z-Fe is the most efficient material for the removal of Cr(VI) present in wastewater.

### ACKNOWLEDGEMENTS

The financial support of the KSCSTE Research Fellowship from the Kerala State Council for Science, Technology and Environment is gratefully acknowledged.

### CONFLICT OF INTEREST

The authors declare that there is no conflict of interests regarding the publication of this article.

### REFERENCES

1. A. Shanaghi, A.R. Sabour, T. Shahrabi and M. Aliofkhaeze, *Prot. Met. Phys. Chem. Surf.*, **45**, 305 (2009); <https://doi.org/10.1134/S2070205109030071>
2. W. Zhang, L. Zou and L. Wang, *Appl. Catal. A Gen.*, **371**, 1 (2009); <https://doi.org/10.1016/j.apcata.2009.09.038>
3. M. Abbas, *J. Water Reuse Desalin.*, **10**, 251 (2020); <https://doi.org/10.2166/wrd.2020.038>
4. S.Y. Lee and S.J. Park, *J. Ind. Eng. Chem.*, **19**, 1761 (2013); <https://doi.org/10.1016/j.jiec.2013.07.012>
5. S. Riaz and S.J. Park, *J. Ind. Eng. Chem.*, **84**, 23 (2020); <https://doi.org/10.1016/j.jiec.2019.12.021>
6. E.A. Serna-Galvis, J. Silva-Agredo, A.L. Giraldo, O.A. Flórez and R.A. Torres-Palma, *Chem. Eng. J.*, **284**, 953 (2016); <https://doi.org/10.1016/j.cej.2015.08.154>
7. J. Zhang, C. Yang, S. Li, Y. Xi, C. Cai, W. Liu, D. Golosov, S. Zavadski and S. Melnikov, *Nanomaterials*, **10**, 2107 (2020); <https://doi.org/10.3390/nano10112107>
8. Y. Yalçın, M. Kiliç and Z. Çınar, *Appl. Catal. B: Environ.*, **99**, 469 (2010); <https://doi.org/10.1016/j.apcatb.2010.05.013>
9. M. Xing, J. Zhang and F. Chen, *J. Phys. Chem. C*, **113**, 12848 (2009); <https://doi.org/10.1021/jp9034166>
10. H. Khan and I.K. Swati, *Ind. Eng. Chem. Res.*, **55**, 6619 (2016); <https://doi.org/10.1021/acs.iecr.6b01104>
11. E. Petala, M. Baikousi, M.A. Karakassides, G. Zoppellaro, J. Filip, J. Tuèek, K.C. Vasilopoulos, J. Pechousek and R. Zbořil, *Phys. Chem. Chem. Phys.*, **18**, 10637 (2016); <https://doi.org/10.1039/C6CP01013J>
12. S. Mustapha, M.M. Ndamitso, A.S. Abdulkareem, J.O. Tijani, D.T. Shuaib, A.O. Ajala and A.K. Mohammed, *Appl. Water Sci.*, **10**, 49 (2020); <https://doi.org/10.1007/s13201-019-1138-y>
13. A.H. Navidpour, B. Xu, M.B. Ahmed and J.L. Zhou, *Mater. Sci. Semicond. Process.*, **179**, 108518 (2024); <https://doi.org/10.1016/j.mssp.2024.108518>
14. J. Huang, S. Yi, C. Zheng and I.M.C. Lo, *Sci. Total Environ.*, **684**, 351 (2019); <https://doi.org/10.1016/j.scitotenv.2019.05.331>
15. Q. Sun, X. Hu, S. Zheng, Z. Sun, S. Liu and H. Li, *Powder Technol.*, **274**, 88 (2015); <https://doi.org/10.1016/j.powtec.2014.12.052>
16. Y.H. Jan, L.Y. Lin, M. Karthik and H. Bai, *J. Air Waste Manag. Assoc.*, **59**, 1186 (2009); <https://doi.org/10.3155/1047-3289.59.10.1186>
17. D. Mirzaei, A. Zabardasti, Y. Mansourpanah, M. Sadeghi and S. Farhadi, *J. Inorg. Organomet. Polym. Mater.*, **30**, 2067 (2020); <https://doi.org/10.1007/s10904-019-01369-9>
18. K. Kusdianto, M. Hudandini, D. Jiang, M. Kubo and M. Shimada, *Catalysts*, **12**, 17 (2021); <https://doi.org/10.3390/catal12010017>
19. S.M. Baghbanian, *RSC Adv.*, **4**, 59397 (2014); <https://doi.org/10.1039/C4RA10537K>
20. A. Kalantarifard, J.G. Gon and G.S. Yang, *Terr. Atmos. Ocean. Sci.*, **27**, 865 (2016); [https://doi.org/10.3319/TAO.2016.05.28.01\(TT\)](https://doi.org/10.3319/TAO.2016.05.28.01(TT))
21. W. Gao, D. Zhong, Y. Xu, H. Luo and S. Zeng, *J. Dispers. Sci. Technol.*, **43**, 1197 (2020); <https://doi.org/10.1080/01932691.2020.1848583>
22. Y. Sun, B. Yang, Y. Tian, G. Guo, W. Cai, M. He and Y. Liu, *Micro & Nano Lett.*, **6**, 82 (2011); <https://doi.org/10.1049/mnl.2010.0149>
23. S. Sood, A. Umar, S.K. Mehta and S.K. Kansal, *J. Colloid Interface Sci.*, **450**, 213 (2015); <https://doi.org/10.1016/j.jcis.2015.03.018>
24. G. Zhang, A. Song, Y. Duan and S. Zheng, *Micropor. Mesopor. Mater.*, **255**, 61 (2018); <https://doi.org/10.1016/j.micromeso.2017.07.028>
25. S. Bagheri, K. Shamel and S.B. Abd Hamid, *J. Chem.*, **2013**, 848205 (2013); <https://doi.org/10.1155/2013/848205>
26. Y. Rashtbari, J.H.P. Américo-Pinheiro, S. Bahrami, M. Fazlzadeh, H. Arfaeinia and Y. Poureshgh, *Water Air Soil Pollut.*, **231**, 514 (2020); <https://doi.org/10.1007/s11270-020-04872-9>
27. Y. Song, X. Lu, Z. Liu, W. Liu, L. Gai, X. Gao and H. Ma, *Nanomaterials*, **12**, 291 (2022); <https://doi.org/10.3390/nano12020291>